Distinct structural transitions of chromatin topological domains coordinate hormone-induced gene regulation

François Le Dily[1,2,3], Davide Baù[1,3], Andy Pohl[1,2], Guillermo Vicent[1,2], François Serra[1,3], Daniel Soronellas[1,2], Giancarlo Castellano[1,2,4], Roni H.G. Wright[1,2], Cecilia Ballare[1,2], Guillaume Filion[1,2], Marc A. Marti-Renom[1,3,5,*] and Miguel Beato[1,2,*].

[1] Gene Regulacion, Stem Cells and Cancer Program, Centre de Regulació Genòmica (CRG), Barcelona, Spain

[2] Universitat Pompeu Fabra (UPF), Barcelona, Spain

[3] Genome Biology Group, Centre Nacional d'Anàlisi Genòmica (CNAG), Barcelona, Spain

[4] Hospital Clínic, Universitat de Barcelona, Barcelona, Spain

[5] Institució Catalana de Recerca i Estudis Avançats (ICREA), Barcelona, Spain

***corresponding authors**

Miguel Beato	Marc A. Marti-Renom
E-mail: miguel.beato@crg.es	E-mail: mmarti@pcb.ub.cat
Centre de Regulació Genòmica (CRG)	Centre Nacional d'Anàlisi Genòmica (CNAG)
Dr. Aiguader 88,	Baldiri i Reixac 4,
E-08003, Barcelona, Spain.	E-08028, Barcelona, Spain.
Tel +34 93 316 0119	Tel. +34 934 020 542
Fax +34 93 316 0099	Fax. +34 934 037 279

Keywords: Three-dimensional structure of the genome, gene expression, Hi-C, TADs, transcriptional regulation, epigenetic landscape, progesterone receptor.

Running title: Hormone remodels specialized chromatin domains.

Supplementary Material

Table of contents

1. Supplementary Methods

1.1. Hi-C libraries, reads mapping and filtering and generation of contact matrices.

Hi-C libraries from T47D cells treated or not with the Pg analogue R5020 for 60 min were generated according the previously published Hi-C protocol with minor adaptations (Lieberman-Aiden et al. 2009). Hi-C libraries were performed in both conditions using *HindIII* and *NcoI* restriction enzymes to generate two independent biological and technical replicates. Briefly, cells were fixed with 1% formaldehyde during 10 min at room temperature. Cross-linking reactions were stopped by addition of glycine (0.125 M final). Cells were scraped and nuclei were prepared as described previously. Chromatin digestion, labelling and ligation steps were performed according the original protocol (Lieberman-Aiden et al. 2009). After deproteinisation, removal of biotinylated free-ends and DNA purification, Hi-C libraries were controlled for quality and sequenced on an Illumina Hiseq2000 sequencer. Paired-end reads were processed by first aligning to the reference human genome (GRCh37/hg19) using BWA. Reads filtered from the analysis include those that were not uniquely mapped, mapped more than 500 bp from relevant internal restriction sites, had bad sequence quality (*e.g*. 40% or more of the bases with Sanger PHRED quality ≤ 2) or bad BWA mapping quality (≤ 20), or were located in regions classified to have exceptionally high sequence depth (top 0.1%) by the 1000 Genomes project's data. To offset bias introduced by PCR amplification of the sequencing library, only one of the duplicated pairs were used for subsequent analyses. Datasets normalized for sequencing depth and experimental biases (Imakaev et al. 2012) were used to generate contact matrices at 20, 40 and 100 Kb as well as at 1Mb resolutions. The Supplementary table 1 summarizes the number of interactions obtained for each dataset.

1.2. Genome segmentation in TADs.

The genome was segmented in TADs by the TADbit program that includes a change-point algorithm for the detection of TAD borders inspired by methods used to detect copy number variations in CGH experiments (Pique-Regi et al. 2008). Briefly, the optimal segmentation of the chromosome in *k* TADs is

computed by maximum likelihood for every *k*, after which a Bayesian Information Criterion selects the best model. The hypotheses underlying the model are that the number of interactions between two loci has a Poisson distribution, of which the average decreases as a power law function of their separation (in base pairs). Each TAD corresponds to a vertical slice of the Hi-C interaction matrix, where the parameters of the model mentioned above are constant. The parameters are corrected for local biases (most notably G+C content, availability of the restriction enzyme site and repeat coverage) (Imakaev et al. 2012). The detail of the implementation of TADbit will be further detailed elsewhere (Serra et al., manuscript in preparation).

1.3. Epigenetic data collection and analyses.

MNase-seq, DNase I-seq and ChIP-seq experiments (H3K4me1, H3K4me3, H2A, H4, RNA polymerase II, progesterone receptor, H3K9me3, HP1γ) in T47D cells were described previously (Ballare et al. 2013; Vicent et al. 2013). Additional ChIP-seq experiments for CTCF, H3K36me2, H3K27me3, H3K14ac and H1.2 were performed in similar conditions using the following antibodies: 07-729 (Millipore), 07-369 (Millipore) 39155 (Active Motif), 07-353 (Millipore) and ab4086 (Abcam), respectively. All reads were processed by aligning to the reference human genome (GRCh37/hg19). MNase-seq, DNase I-seq and ChIP-seq signals normalised for sequencing depth were summed in windows of 100 Kb. To generate plots in Supplementary Figures 2 and 3, bins correspond to a fifth of the TAD size (hereafter mentioned as sub-segments). Summed reads for these different window sizes were divided by the corresponding signal obtained for an input DNA of T47D cells to determine the normalised signal over input enrichment/depletion. Progesterone-induced enrichment or depletion of mark content were determined for 100 Kb bins or for the whole TAD as the ratio of sequencing-depth normalised read counts before and after treatment.

1.4. Role of TAD borders in demarking chromatin blocks.

To analyse the role of the TAD borders in limiting epigenetic blocks of individual marks, the opposite of the absolute difference of the signals, normalised as above, was calculated for two consecutive sub-segments (with each TAD divided into 5 segments of equal size) on 3 consecutive TADs. Therefore, the

higher the score is, the more similar the signals between consecutive segments. These scores were computed genome-wide, and the quartiles of the 14 consecutive values were calculated to generate the plots in Supplementary Fig. 3a and c. To control that the observed differences were not due to biases in the sizes of the sub-segment, and to confirm the role of the TAD borders, we shuffled the TADs chromosome-wise. As a robust control which conserves both size and sequences of genomic domains, random segmentations of the genome included inversion of the position of TADs from telomere to centromere on each chromosomal arm (mentioned as random genomic domains (random GD) in the main text and figures).

To analyse the homogeneity of epigenetic marks within TADs, we generated pairwise correlation matrices between the profiles of the marks described above for all 100 Kb windows of the genome. From this, we computed the average correlation between 100 Kb windows located in the same TAD. If TADs are homogeneous in chromatin marks combinations, this average correlation will be higher than expected by chance. To estimate the null distribution of this score, we shuffled the TADs chromosome-wise 5,000 times and applied the same procedure. The average correlation obtained with the initial positions of the TADs was higher than the average correlation when the TADs were randomized. Finally, we repeated the same analysis using the differential of the normalised signal after treatment with R5020 and the signal before treatment.

Borders of epigenetic domains were defined applying Principal Component Analysis to the pair-wise correlation matrices of epigenetic profiles between 100 kb windows of the chromosomes obtained above. The number of those borders that were located from 0 to 500 Kb from the TADs border were computed and compared to random segmentation of the genome (see above).

1.5. Expression levels (RNA-seq) and hormone-induced changes.

RNA-seq experiments were performed in T47D treated or not with 10^{-8} M R5020 (Pg) for 1 or 6 h or with 10^{-8} M estradiol (E2) for 6 h. Paired-end reads were mapped with the GEM mRNA Mapping Pipeline (v1.7) (Marco-Sola et al. 2012) using the latest gencode annotation version (v.18) (Harrow et al. 2012). BAM

alignment files were obtained and used to generate strand-specific genome-wide normalized profiles with RSeQC (Wang et al. 2012) software. Exon quantifications summarized per gene for expression level determination were obtained either as normalised read counts or reads per kilobase per milion mapped reads (RPKM) using Flux Capacitor (Montgomery et al. 2010). Fold changes (FC) were computed as the $\log_2$ ratio of normalised reads per gene obtained after and before treatment with hormones. Genes with fold-change ± 1.5 (p-value < 0.05 ; FDR < 0.01) were considered as significantly regulated.

To analyse the changes of non-protein coding regions of the genome, the number of normalised reads were computed independently for chromosomal fractions of the TAD that do not overlap with any annotated protein-coding gene and for chromosomal fractions of the TAD which contained protein-coding reads.

In order to compare the observed and expected number of genes positively or negatively affected by hormone treatment and to exclude potential biased responses depending on low/high basal expression of genes, randomizations of protein-coding gene positions used in Figure 2F were obtained as follow: genes were classified in 5 classes of equivalent sizes according their expression level. Gene positions were then shuffled for the 5 classes allowing conserving an equivalent average expression of genes per TAD. Shuffled lists were then used to calculate the percentage of genes with positive or negative fold change per TAD and compared to the observed distribution.

1.6. Classification of TAD according transcriptional response to Pg.

To classify TADs according their hormone response, we calculated the average ratio of the number of RNA-seq reads normalized for sequencing depth obtained after and before hormone treatment in the RNA-seq replicates. TADs containing more than 3 protein coding genes were saved for further analysis and ranked according to the average ratio described above. The top and bottom 100 were classified as “activated” and “repressed” TADs, respectively. Similar classifications were performed for Pg and E2 response.

1.7. Fluorescent in situ hybridization.

T47D cells grown on slides were fixed with 4% paraformaldehyde in PBS 15 min at room temperature. After washes with PBS and permeabilisation with 0.2% Triton X-100 in PBS, slides were incubated 60 min with RNase A in SSC2X. Fixed cells were incubated 3 min in 0.1 N HCl and 1 min in 0.01 N HCl with 0.01% pepsin. Slides were denatured at 70ºC for 8 min in SSC 2×-70% formamide and incubated overnight at 37ºC in a humid chamber with the probes (separately denatured 10 min at 80ºC in hybridization buffer). 100 ng of each probe generated by nick translation using dUTP-biotin, dUTP-DIG and dUTP-fluorescein (Roche Applied Biosciences) was used per hybridization. Detection was performed with ant-biotin-Cy5 (Rockland), anti-DIG-rhodamin (Roche) and anti-fluorescein-Alexa 488 (Invitrogen). Machine optimized stacks were acquired on a Zeiss TCS SP5 confocal microscope. After deconvolution, 3D rendering of the hybridised probes signals were generated for each channel, and the pair-wise 3D distances between the centre of mass of these signals were computed using the Imaris Software.

The BACs used in this study were obtained from a 32k library:

RP11-758G19	chr1	:	26742822	-	26905278
RP11-443P17	chr1	:	26877973	-	27069024
RP11-973A19	chr1	:	27772963	-	27993702
RP11-667P18	chr1	:	28384701	-	28571122
RP11-318E23	chr1	:	28980912	-	29129694
RP11-476G18	chr2	:	43138737	-	43367330
RP11-525B14	chr2	:	43696249	-	43835952
RP11-4K20	chr2	:	11054580	-	11235239
RP11-345J13	chr2	:	11204622	-	11377387
RP11-487B6	chr2	:	11519339	-	11687756
RP11-641J22	chr2	:	11624003	-	11836772

1.8. Integrative 3D modelling of TADs.

Hi-C data matrices

Hi-C experimental data resulted in interaction counts between the loci of the

genomic region of interest (*i.e.* the quantitative determination of the number of times each specific experimental ligation product is sequenced). We then applied an internal normalization by Z-scoring the sequenced raw interaction count data. First, we applied a log2 transformation of the raw counts and then their Z-score was calculated as: $Zscoreij = \frac{Cij-\mu}{\sigma}$; where μ and σ are the average and standard deviation of the interaction counts for the entire Hi-C matrix. Such normalization allowed us to quantify the variability within the Hi-C matrix as well as to identify pairs of fragments that significantly interacted above or below the average interaction frequency.

TAD representation

Hi-C datasets obtained with *HindIII* and *NcoI* enzymes were pooled to generate normalized Hi-C matrices at 20 Kb resolution. Consequently, each modelled genomic region was represented as a set of particles, one per each 20 Kb bin. Each particle had a radius of 100 nm, based on the relationship of 0.01 nm per base pair (bp)(Harp et al. 2000). Neighbour particles were constrained to lie at an equilibrium distance proportional to the sum of their excluded volume. Non-neighbor particle pairs (*i.e.* particles representing non-consecutive bins along the genomic sequence) were instead assigned a distance derived from the z-score matrices. The function mapping the z-scores onto distances was defined as the calibration curve built by interpolating the highest and the lowest z-score values, with a minimum proximity distance of 200 nm (the excluded volume of two base particles) and a maximal proximity distance for two non-interacting fragments, respectively, as previously described (Bau and Marti-Renom 2012). The forces applied to the defined restraints were also set proportionally to the absolute value of the Hi-C z-score observed between a pair of fragments.

TAD modelling

Each particle pair was restrained by a series of harmonic oscillator centred on a distance derived from the experimental data. Consecutive particles (*i.e*. particle pairs —or bins— *i, i+1*) were considered as neighbour particles and therefore retrained at an equilibrium distance proportional to the sum of their excluded volume. Non-neighbour particles (*i.e.* particle pairs —or bins— *i, i+2..n*) were

instead restrained at distances calculated from a function that mapped their corresponding z-scores onto distances. This function corresponded to a calibration curve that was built between the points defined by the maximum and minimum z-score values, and two empirically determined minimum and maximum distances, respectively. The maximum distance for non-interacting loci was independently optimized for each modelled region (Supplementary Table 2). Consecutive particles were restrained by an upper-bound harmonic oscillator, which ensured that two particles could not get separated beyond a given equilibrium distance proportional to the sum of their excluded volume. Non-consecutive particles were restrained by two different oscillators: (i) an harmonic oscillator, which ensured a pair of particles to lie at about a given equilibrium distance and (ii) lower-bound harmonic oscillator, which ensured that two particles could not get closer than a given equilibrium distance. In both cases the equilibrium distance was derived by a calibration curve defined by the points corresponding to the maximum and minimum z-score values with a minimum and a maximum distance (see below). The different type of oscillator applied depended on an upper (*uZ*) and a lower (*lZ*) z-score cut-off as well as the approximation distance between two non-interacting particles (*aD*), as previously described (Bau and Marti-Renom 2012). The values of *uZ*, *lZ* and *aD* were independently optimized for each modelled region (Supplementary Table 2).

Neighbour particles were constrained by an upper-bound harmonic oscillator centered at an equilibrium distance proportional to the sum of their excluded volume. Non-neighbour particles with a z-score higher than the upper-bound cut-off (*uZ*) were restrained by a harmonic oscillator, while pairs of particles with a z-score lower than the lower-bound cut-off (*lZ*) were restrained by a lower-bound harmonic oscillator. Since these two harmonic oscillator aim at keeping a pair of particles at an equilibrium distance or further apart from a minimal distance, respectively, pairs of non-neighbour particles that were observed to interact with z-scores above the *uZ* parameter were kept close in space, while pairs of non-neighbor particles that were observed to interact with z-scores below the *lZ* parameter were kept apart. The *k* force applied to these restraints was set to the square root of the absolute value of their interacting z-scores. Finally, pairs of non-neighbour particles for which Hi-C data were not available

were restrained based on the average z-score of the adjacent particles.

Model building with IMP

Following the steps previously described (Bau and Marti-Renom 2012), we modelled the 3D structure of 61 genomic regions. The selected regions included a total of 209 TADs and covered about 267 Mb of the genome (Supplementary Table 3). Once the system was fully represented and the restraints between the particles were set, IMP generated the ensemble of solutions that best represented the input data by simultaneously minimizing the violations of all the imposed restraints. Due to the large conformational space to be explored and to the population-based nature of 3C-based methods, the optimization of the imposed restraints resulted in different configurations with similar final IMP objective function. Thus, to comprehensively explore the conformational space of the modelled TADs, we generated a large number of models for each conditions (2,000 models for each) by globally minimizing the imposed restraints via a combination of 10,000 Monte Carlo rounds with 5 local steps in a molecular dynamics simulation with a standard simulated annealing method. At each optimization step, the conformation was randomly changed and the change was accepted or rejected according to the Metropolis criteria. The driving scoring function that was minimized during the optimization protocol consisted of the sum of all the individual restraint scores between all the particles representing the system. The entire calculation of 122 independent simulations resulting in 244,000 different conformational solutions (2,000 for each region and hormone treatment), took about 6 days on a 200 CPU cluster computer.

Model analysis

To further characterize the structural perturbations on TADs by the treatment with Pg, we performed a series of computational analysis in a set of 1,000 selected models with the lowest IMP objective function, which correspond to the 3D models that best satisfy the initial imposed restraints (Bau and Marti-Renom 2012).

The entire set of analysis included:

a) Structural clustering of models.

To structurally compare two 3D models, we used pair-wise rigid-body superposition minimizing the root mean square deviation between the superposed conformations. The comparison resulted in a 1,000×1,000 symmetric matrix of all-against-all structural comparisons storing the number of particles for every pair of aligned models that align within 75 nm distance cut-off. The comparison matrix was then used as input file to the Markov Cluster Algorithm (MCL) program (Enright et al. 2002), which generated unsupervised sets of clusters of related structures.

b) TAD radius of gyration.

The radius of gyration of an object (in our case a TAD) is root mean square distance of the objects' parts from its centre of gravity. We calculated for each TAD a centre of gravity and then measured the distance of all points in the TAD to this centre. The average value of the distances corresponded to the TAD radius of gyration. The larger the radius of gyration is, the more open the TAD is.

c) TAD and particle accessibility.

The particle accessibility of a model is the accessible fraction of its particle to a hypothetical spherical object of a given radius (in our calculations 75 nm). To obtain such fraction, we first build a mesh of points surrounding each particle in the model, which indicates its theoretical occupancy. Then, the spherical object is placed on all possible positions in contact with the model and the fraction of the mesh around the particle that is can be occupied by the object is considered accessible. The accessibility change for a given TAD was calculated as the ratio of the sums of all particle accessibilities in the TAD before and after Pg.

d) Ensemble visualization

The UCSF Chimera package (Yang et al. 2012), a highly extensible program for interactive visualization of molecular structures, was used to produce all images of the modelled TADs.

2. Supplementary Tables

Supplementary Table 1: Summary statistics Hi-C datasets

	HindIII -Pg	HindIII +Pg	NcoI -Pg	NcoI +Pg
Sequenced Fragments Pairs	189563259	146045810	186633896	232632568
Interacting Fragments Pairs*	74015388	48530773	100262904	120640304
"Intra-chromosomal"	29552177	19519911	49163452	57721468
"Inter-chromosomal"	44463211	29010862	51099452	62918836

*: after mapping and filtering

Supplementary Table 2: Summary statistics ChIP-Seq

	Number of reads used	
	-Pg	+Pg
H3K36me2	146,044,735	145,305,602
H3K27me3	133,187,068	279,401,384
H3K14ac	137,810,982	129,554,661
H1.2	148,312,436	146,986,880
H3K4me3	10,065,189	11,640,484
H3K9me3	120,644,215	137,267,014
H3K4me1	163,510,840	143,927,035
H2A	172,656,149	162,799,321
H4	102,527,573	104,886,509

Supplementary Table 3: Summary statistics RNA-Seq

Sample		Mapped reads
T0	BR1	55,552,214
	BR2	77,414,870
	BR3	82,211,476
R1	BR1	60,655,328
	BR2	87,023,754
	BR3	79,338,180
R6	BR1	65,732,986
	BR2	79,752,962
	BR3	88,115,348
E6	BR1	59,466,867
	BR2	92,686,667
	BR3	74,054,115

Supplementary Table 4: IMP optimal modelling parameters

Region	Chrom	Start bin	End Bin	uZ	lZ	aD	CC
1	1	10501	10661	600	0	0	0.74
2	1	11316	11591	400	0	-1.2	0.73
3	1	1816	1926	600	0.6	-0.9	0.75
4	1	3016	3201	400	0.9	-1.2	0.68
5	1	5831	6001	400	0.3	-0.6	0.71
6	1	8376	8576	400	0.3	-1.2	0.70
7	1	9071	9316	400	0.9	-1.2	0.72
8	2	11026	11241	400	0	-0.3	0.65
9	2	2106	2291	600	0	-1.2	0.71
10	2	3481	4011	400	0	0	0.63
11	2	481	661	400	0	-1.2	0.73
12	2	7911	8046	400	0	-1.2	0.69
13	2	9941	10131	400	0	-1.2	0.68
14	3	7516	7921	600	0.9	-0.6	0.65
15	3	8396	8501	700	0.6	-0.6	0.77
16	4	1971	2101	400	0	-0.6	0.71
17	4	356	491	700	0.3	0	0.73
18	4	3991	4166	400	0	-0.6	0.62
19	4	4411	4761	400	1.2	-1.2	0.59
20	4	5246	5481	400	0.3	-0.6	0.63
21	5	2606	2916	500	0	-1.2	0.72
22	5	536	811	500	0	-1.2	0.66
23	5	7051	7406	600	0.9	-0.3	0.67
24	6	2681	3201	600	0.3	0	0.65
25	6	3591	3826	700	0	-1.2	0.67
26	6	7561	7666	700	0.6	0	0.64
27	6	7886	8056	600	0.3	-1.2	0.62
28	7	2411	2741	500	0.6	-0.6	0.64
29	7	4391	4611	400	0.9	-1.2	0.63
30	7	7831	7961	400	0	-0.9	0.72
31	8	2676	2851	400	0	-0.6	0.73
32	8	456	596	600	0.3	-0.3	0.70
33	8	5196	5346	600	0	-0.3	0.71
34	9	1	106	600	0.3	-0.6	0.71
35	9	5856	6241	400	0	-0.6	0.69
36	9	6961	7066	500	0	-0.9	0.84
37	10	1066	1546	600	0	-1.2	0.64
38	10	2596	2726	600	0.6	-0.6	0.69
39	10	296	471	600	0	-0.3	0.73
40	10	3851	4066	600	0.6	0	0.77
41	10	4721	4846	700	0.6	-0.3	0.80
42	11	3716	4121	400	0	-0.9	0.67
43	12	1556	1721	400	0	-0.9	0.70
44	12	4471	4656	600	0.9	-0.6	0.69
45	12	5116	5291	600	0.3	-0.6	0.76
46	12	806	1076	400	0.6	-1.2	0.61
47	13	1196	1306	500	0	-0.6	0.73

48		13	1981	2306	400	0.9	-1.2	0.64
49		13	5176	5561	400	0	-0.9	0.64
50		14	3091	3241	500	0.6	-0.6	0.69
51		14	4446	4596	400	0	-1.2	0.72
52		15	4991	5131	700	0.3	-0.3	0.76
53		16	3866	4121	400	0.3	-0.3	0.69
54		18	771	1191	400	1.2	-1.2	0.68
55		20	1571	1671	500	0.3	-1.2	0.77
56		21	1406	1626	400	0	-1.2	0.65
57		21	1746	1921	700	0	0	0.76
58		21	2031	2241	600	0.9	-0.6	0.75
59	X		6471	6576	400	0	-0.6	0.68
60	X		6861	6991	400	0	-0.9	0.59
61	X		791	936	400	0.9	-1.2	0.74

CC corresponds to the correlation coefficient of a contact map based on the 3D models and the input HiC data for the region. High correlation coefficients are indicative of the bona fide representation of the HiC data by the models.

3. Supplementary References

Ballare C, Castellano G, Gaveglia L, Althammer S, Gonzalez-Vallinas J, Eyras E, Le Dily F, Zaurin R, Soronellas D, Vicent GP et al. 2013. Nucleosome-driven transcription factor binding and gene regulation. *Molecular cell* **49**: 67-79.

Bau D, Marti-Renom MA. 2012. Genome structure determination via 3C-based data integration by the Integrative Modeling Platform. *Methods* **58**: 300-306.

Enright AJ, Van Dongen S, Ouzounis CA. 2002. An efficient algorithm for large-scale detection of protein families. *Nucleic acids research* **30**: 1575-1584.

Harp JM, Hanson BL, Timm DE, Bunick GJ. 2000. Asymmetries in the nucleosome core particle at 2.5 A resolution. *Acta crystallographica Section D, Biological crystallography* **56**: 1513-1534.

Harrow J, Frankish A, Gonzalez JM, Tapanari E, Diekhans M, Kokocinski F, Aken BL, Barrell D, Zadissa A, Searle S et al. 2012. GENCODE: the reference human genome annotation for The ENCODE Project. *Genome research* **22**: 1760-1774.

Imakaev M, Fudenberg G, McCord RP, Naumova N, Goloborodko A, Lajoie BR, Dekker J, Mirny LA. 2012. Iterative correction of Hi-C data reveals hallmarks of chromosome organization. *Nature methods* **9**: 999-1003.

Lieberman-Aiden E, van Berkum NL, Williams L, Imakaev M, Ragoczy T, Telling A, Amit I, Lajoie BR, Sabo PJ, Dorschner MO et al. 2009. Comprehensive mapping of long-range interactions reveals folding principles of the human genome. *Science* **326**: 289-293.

Marco-Sola S, Sammeth M, Guigo R, Ribeca P. 2012. The GEM mapper: fast, accurate and versatile alignment by filtration. *Nature methods* **9**: 1185-1188.

Montgomery SB, Sammeth M, Gutierrez-Arcelus M, Lach RP, Ingle C, Nisbett J, Guigo R, Dermitzakis ET. 2010. Transcriptome genetics using second generation sequencing in a Caucasian population. *Nature* **464**: 773-777.

Pique-Regi R, Monso-Varona J, Ortega A, Seeger RC, Triche TJ, Asgharzadeh S. 2008. Sparse representation and Bayesian detection of genome copy number alterations from microarray data. *Bioinformatics* **24**: 309-318.

Vicent GP, Nacht AS, Zaurin R, Font-Mateu J, Soronellas D, Le Dily F, Reyes D, Beato M. 2013. Unliganded progesterone receptor-mediated targeting of an RNA-containing repressive complex silences a subset of hormone-inducible genes. *Genes & development* **27**: 1179-1197.

Wang L, Wang S, Li W. 2012. RSeQC: quality control of RNA-seq experiments. *Bioinformatics* **28**: 2184-2185.

Yang Z, Lasker K, Schneidman-Duhovny D, Webb B, Huang CC, Pettersen EF, Goddard TD, Meng EC, Sali A, Ferrin TE. 2012. UCSF Chimera, MODELLER, and IMP: an integrated modeling system. *Journal of structural biology* **179**: 269-278.

4. Supplementary Figures and legends

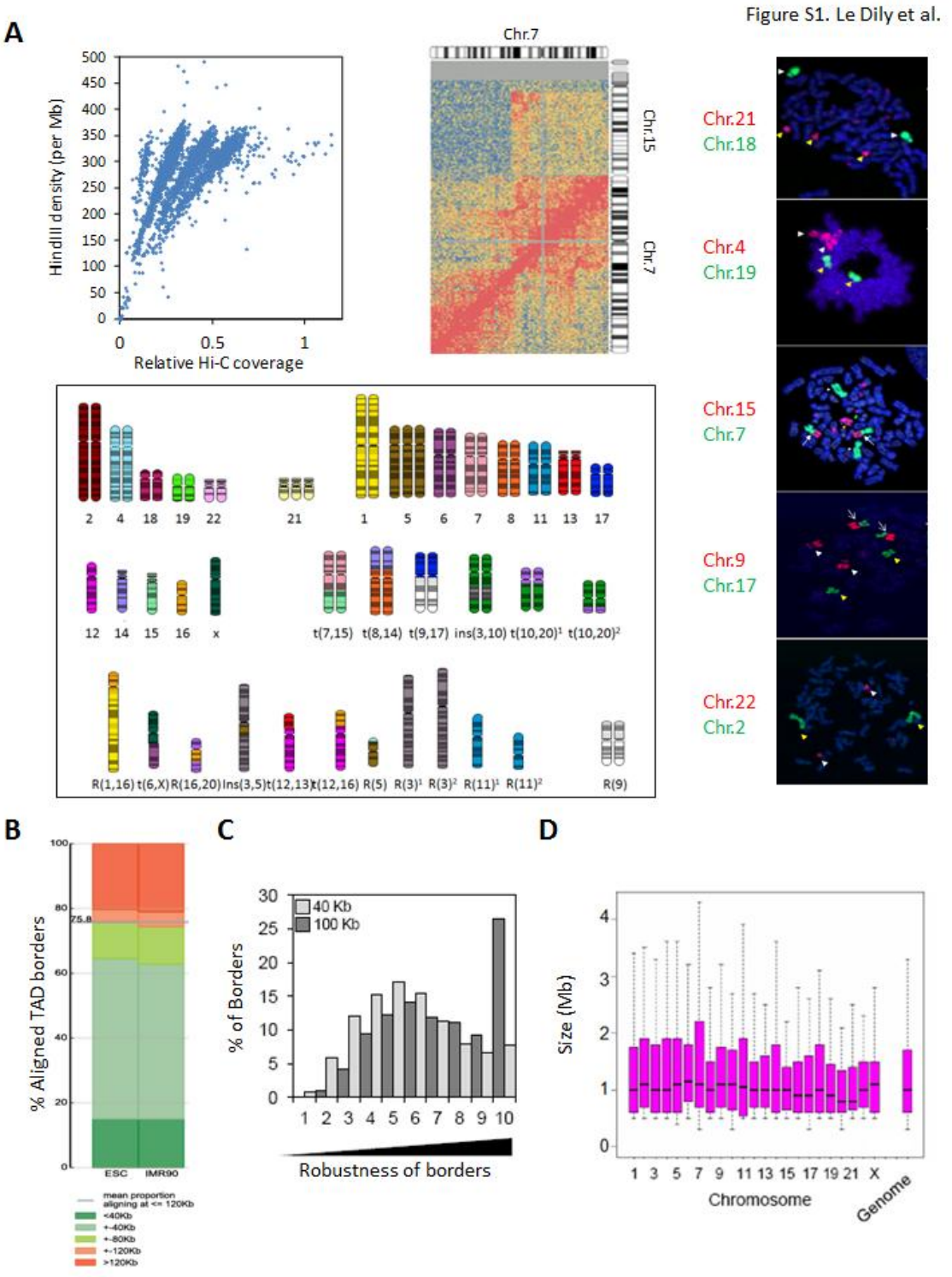

Supplementary Figure 1: T47D genome is organised in TADs.

(A) The linear correlation between number of Hi-C contacts and number of restriction sites is lost due to changes in copy number allowing determining the number of copies of each megabase domains present in T47D genome (top left

panel). A snapshot of contact matrix shows an example of translocation breackpoint between the chromosomes 7 and 15 in T47D cells (top middle panel). T47D karyotype deduced from the variations in copy number and translocations events determined as above is represented (bottom panel). Left panel show examples of 2D-FISH on T47D cells metaphase spreads validating the karyotype and highlighting changes in ploidy, translocation events as well as normal chromosomes. **(B)** Plot showing the correspondence of TADs borders defined in ESC and IMR90 cells by Dixon et al. and by the approach described in this study (See Supplementary Methods). **(C)** Distribution of boundaries confidence scores for TADs defined at 40 (light grey – n=3027) or 100 Kb (dark grey – n=2031) resolutions. **(D)** Distribution of TAD sizes determined at 100 Kb resolution (N genome=2031).

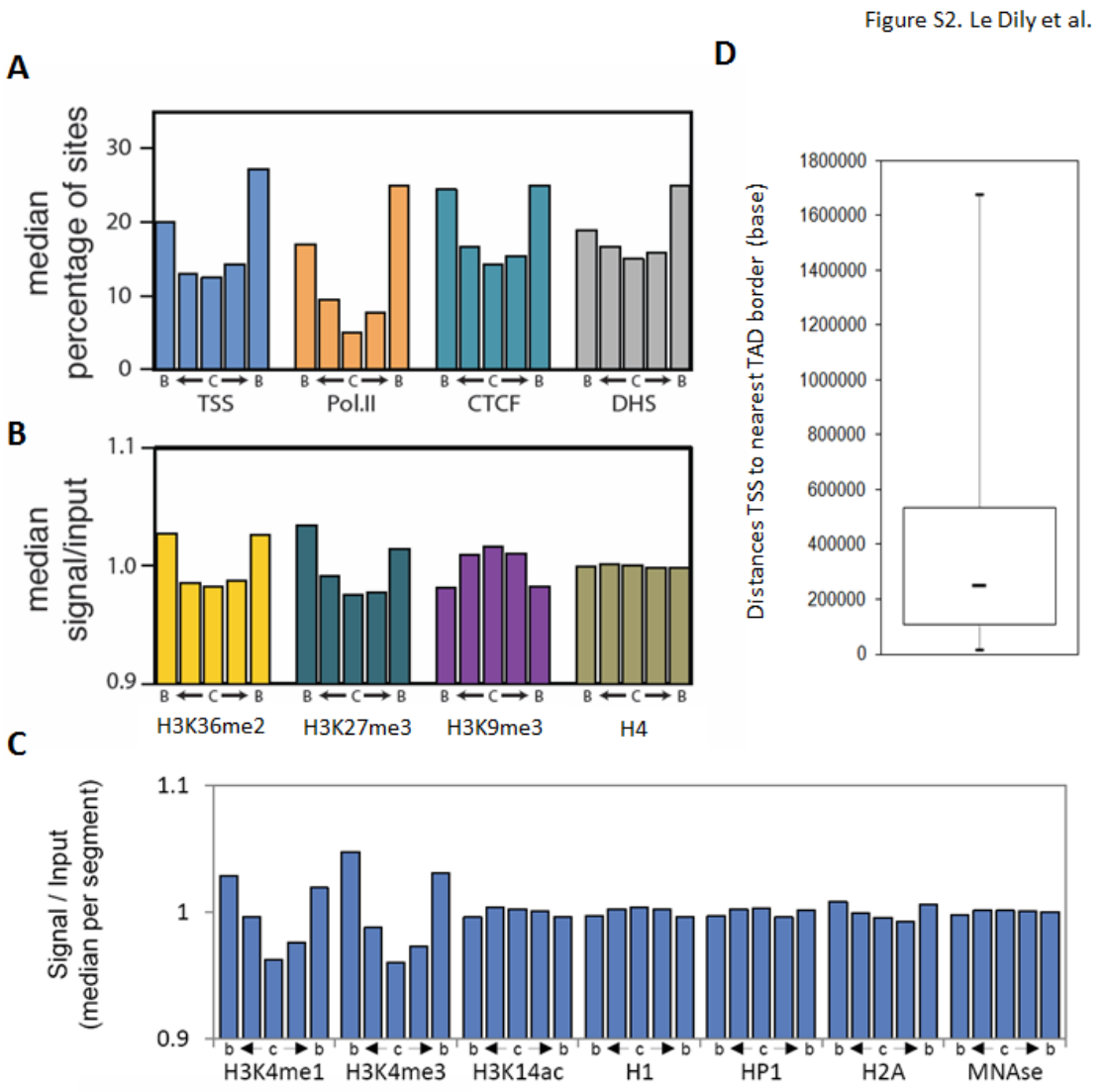

Supplementary Figure 2: Functional characterization of TADs.
TADs were divided into 5 sub-segments of equal size to study the distribution of epigenetic features according a border (b) to center (c) distribution (see Supplementary Methods). **(A)** The median percentage of Transcription Start Sites of protein coding genes (TSS), RNA-Polymerase II (Pol.II), and CTCF binding sites, as well as DNAse I hypersensitive sites (DHS) is shown. **(B)** The histogram represent the median ratio of normalised ChIP-Seq signals over input for H3K36me3, H3K27me3, H3K9me3 and total H4 determined in the TADs 5 sub-segments. **(C)** Normalised ChIP-Seq signals over input ratio were calculated per sub-segment for each TAD for the indicated chromatin components and marks mentioned. Histograms show, for each mark, the median normalised signal/Input observed in the 5 sub-segments for all TADs in the genome. **(D)** Distributions of the distances between Transcription Start Sites (TSS) of protein coding genes to the nearest TADs border in base.

Figure S3. Le Dily et al.

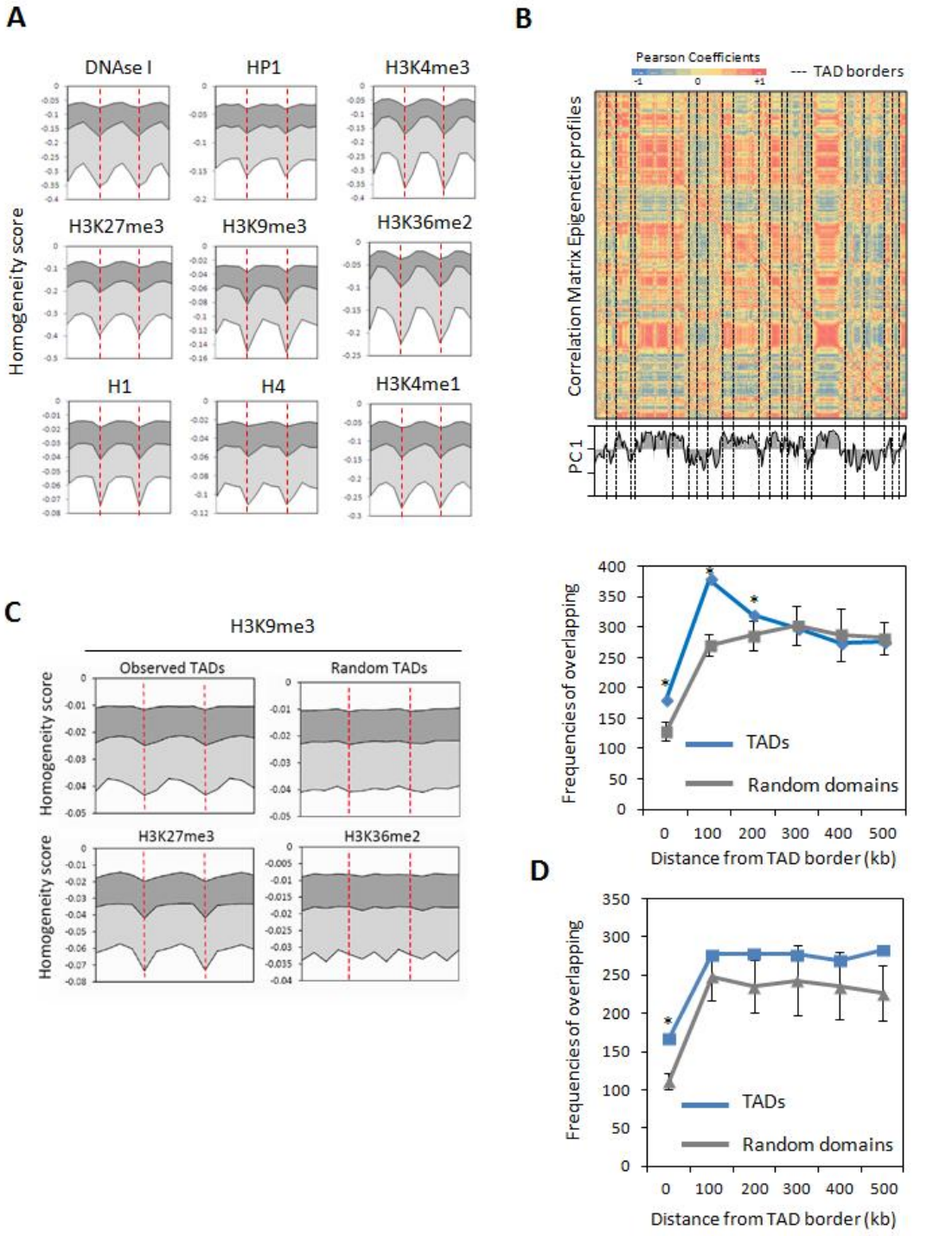

Supplementary Figure 3: TADs are epigenetic domains which chromatin is coordinately modified upon Pg.

(A) Plots show the homogeneity score of the normalised Chip-Seq signal/Input ratio between successive sub-segments (see Supplementary Methods) over 3 consecutive TADs for the chromatin marks and components listed. Lines depict the 25th, 50th and 75th percentiles (from top to bottom respectively) of the scores computed genome-wide. The red dashed lines correspond to the TADs borders.

(B) Pearson Correlation Coefficient of the combinations of epigenetic marks were calculated pair-wise in order to generate correlation matrices between 100Kb windows of the genome. Upper panel shows example of such matrices obtained for the region of chromosome 2 presented in Fig. 2. Location of the TADs borders are represented by the black dashed lines. These matrices were submitted to Principal Component Analysis and the first component (PC1) was used to delimit epigenetic domains. Genome wide, 1812 epigenetic domains borders were identified and the number of those borders located at increasing distances from TADs borders or random genomic borders were computed (Bottom panel). **(C)** Differences of +Pg/-Pg H3K9me3 Chip-Seq signal between consecutive sub-segments (see Fig. S3 and Supplementary information) over 3 consecutive TADs in the case of observed (*left panel*) or randomized (*right panel*) TADs borders show that transition between Pg induced changes in chromatin state occur preferentially at the TAD boundaries. Similar analysis was performed for other chromatin marks as example H3K27me3 and H3K36me2. The red dashed lines correspond to the TADs borders. **(D)** Similar analysis as described in B was applied using the correlation between the profiles of Pg-induced changes on chromatin.1695 domains of correlated changes were identified and their borders and the number of those borders located at increasing distances from TADs borders or random borders were computed.

Figure S4. Le Dily et al.

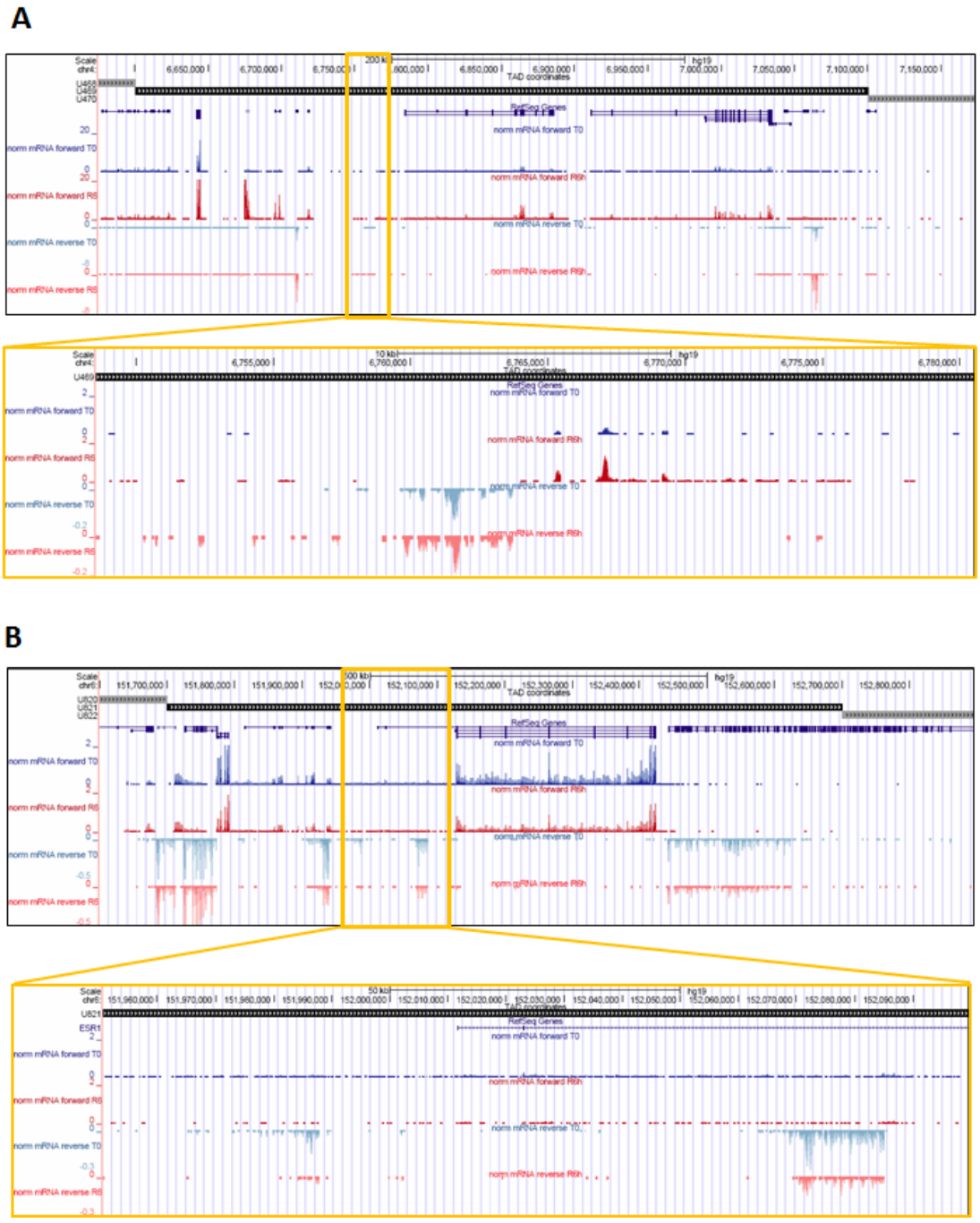

Supplementary Figure 4: TADs respond as unit to the hormone stimulus
(A and B) Genome browser view of RNA-Seq signal within TADs presented in Figure 2E (**(A)** U469; **(B)** U821) highlighting the expression of non-annotated non-coding transcripts which correlate with the hormone induced changes in expression observed for the protein coding genes.

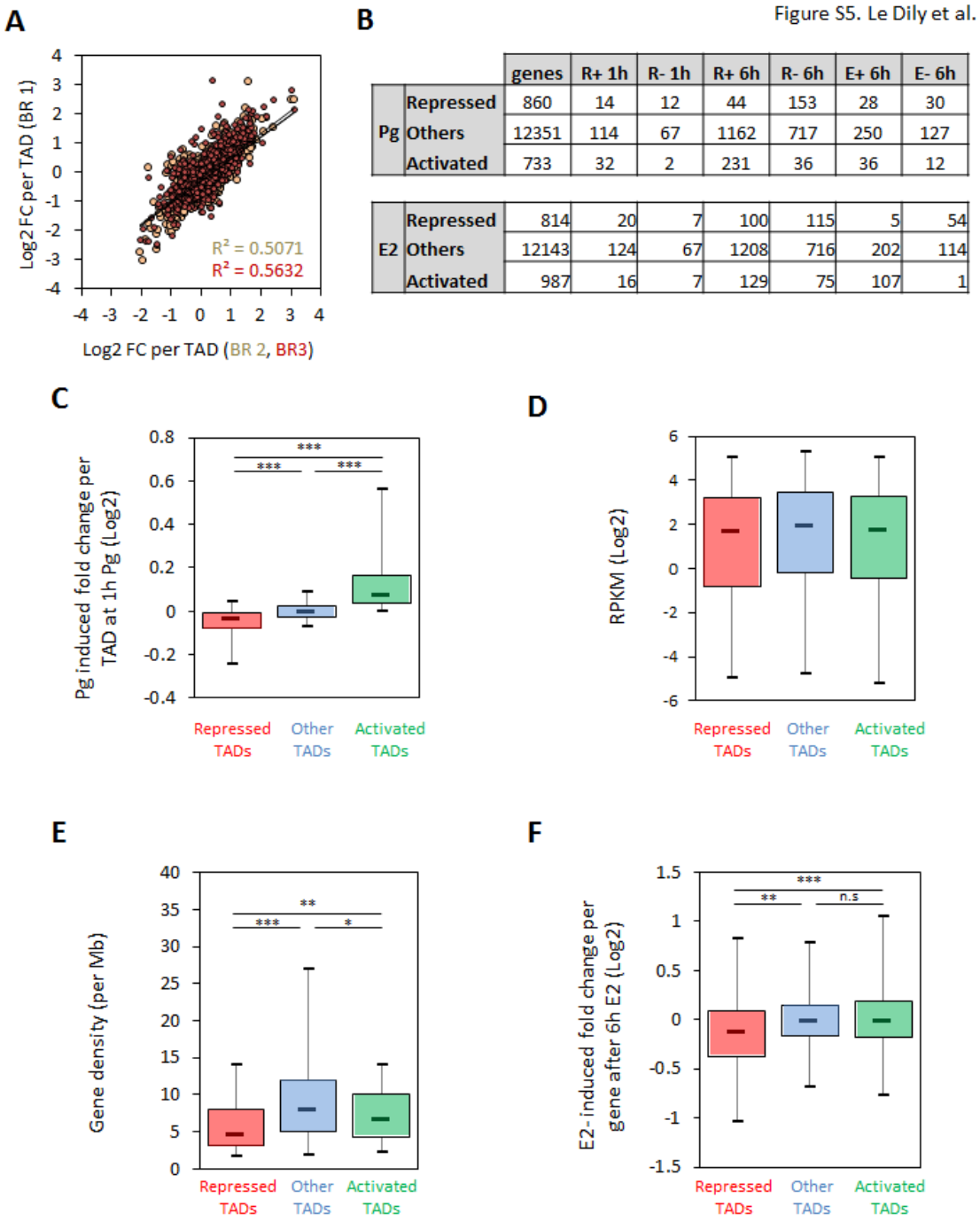

		genes	R+ 1h	R- 1h	R+ 6h	R- 6h	E+ 6h	E- 6h
Pg	Repressed	860	14	12	44	153	28	30
	Others	12351	114	67	1162	717	250	127
	Activated	733	32	2	231	36	36	12
E2	Repressed	814	20	7	100	115	5	54
	Others	12143	124	67	1208	716	202	114
	Activated	987	16	7	129	75	107	1

Supplementary Figure 5: Homogeneous and specific response of TADs to steroid hormones.

(A) The ratio of normalised reads after and before 6 hour of treatment with Pg were calculated for each TAD. The scatter plot shows the correlation of response to Pg per TAD obtained between biological replicates (BR1 against BR2 and BR3) of RNA-Seq. **(B)** The table depicts the number of genes found significantly regulated after 1h or 6h of treatment with Pg and 6h of treatment with E2 within the different types of TADs classified according their Pg or E2 response. (R+: Pg-Up-regulated genes, R-: Pg-Down-regulated genes, E+: E2-Up-regulated genes, E-: E2-Down-regulated genes). **(C)** Distributions of Pg-

induced fold changes of expression per TAD after 1h of treatment with Pg according their type defined at 6h. **(D)** Boxplots show the basal expression levels (RPKM – Log_2) of genes located within the three types of TADs. **(E)** Distributions of the TADs gene densities according the type of TADs. **(F)** Distributions of E2-induced fold changes (6h) of expression of genes located in the different types of Pg responsive TADs. Boxplot whiskers correspond to 5^{st} and 95^{th} percentiles. (***),(**),(*) indicate P < 0.001, 0.01 and 0.05, respectively (Bonferroni corrected Mann-Whitney test).

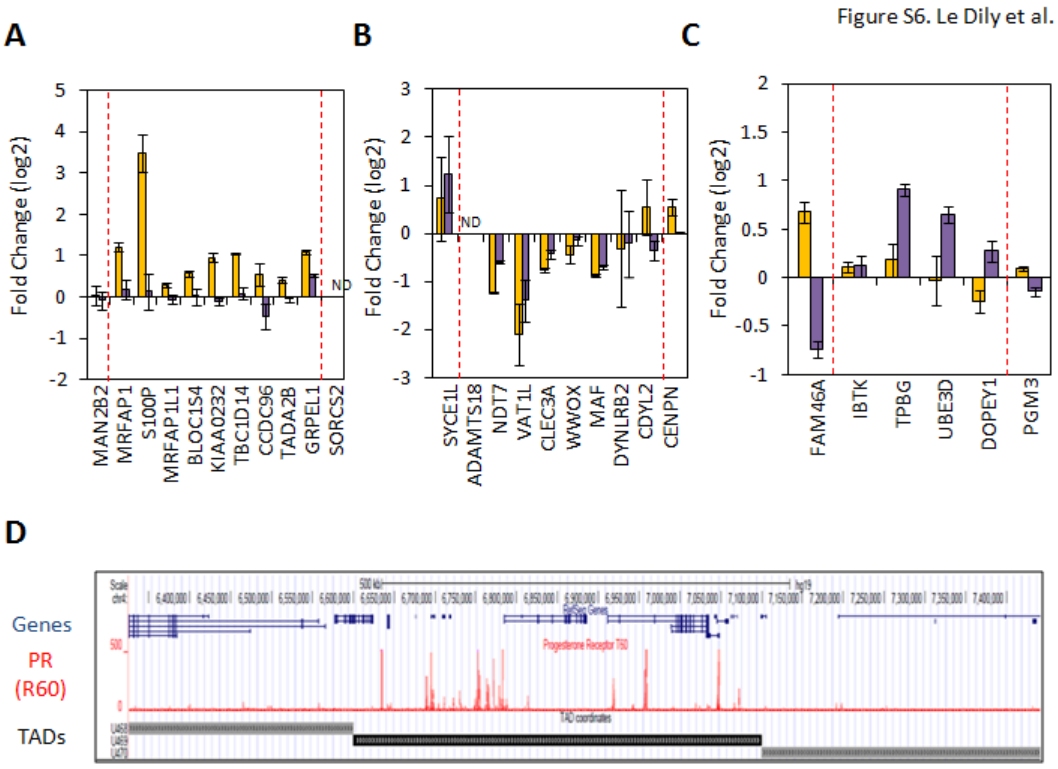

Supplementary Figure 6: TADs respond differentially to distinct stimuli.
(A, B, C) Example of TADs with biased coordinated response to Pg and/or E2. Panels show the $\log_2$ ratio of expression of individual genes obtained after a 6h treatment with Pg (yellow) or E2 (purple). (ND: Not detected). (A): TAD 469 -- Chr.4:6,600,000-7,100,000 (results of Pg response are also shown in Fig. 2 E).; (B): TAD 1666 – Chr.16:77,300,000-81,000,000; (C) TAD772 – Chr.16:82,900,000-83,800,000 **(D)** Genome browser view of the density of PR binding within an activated TADs (TAD 469 -- Chr.4:6,600,000-7,100,000).

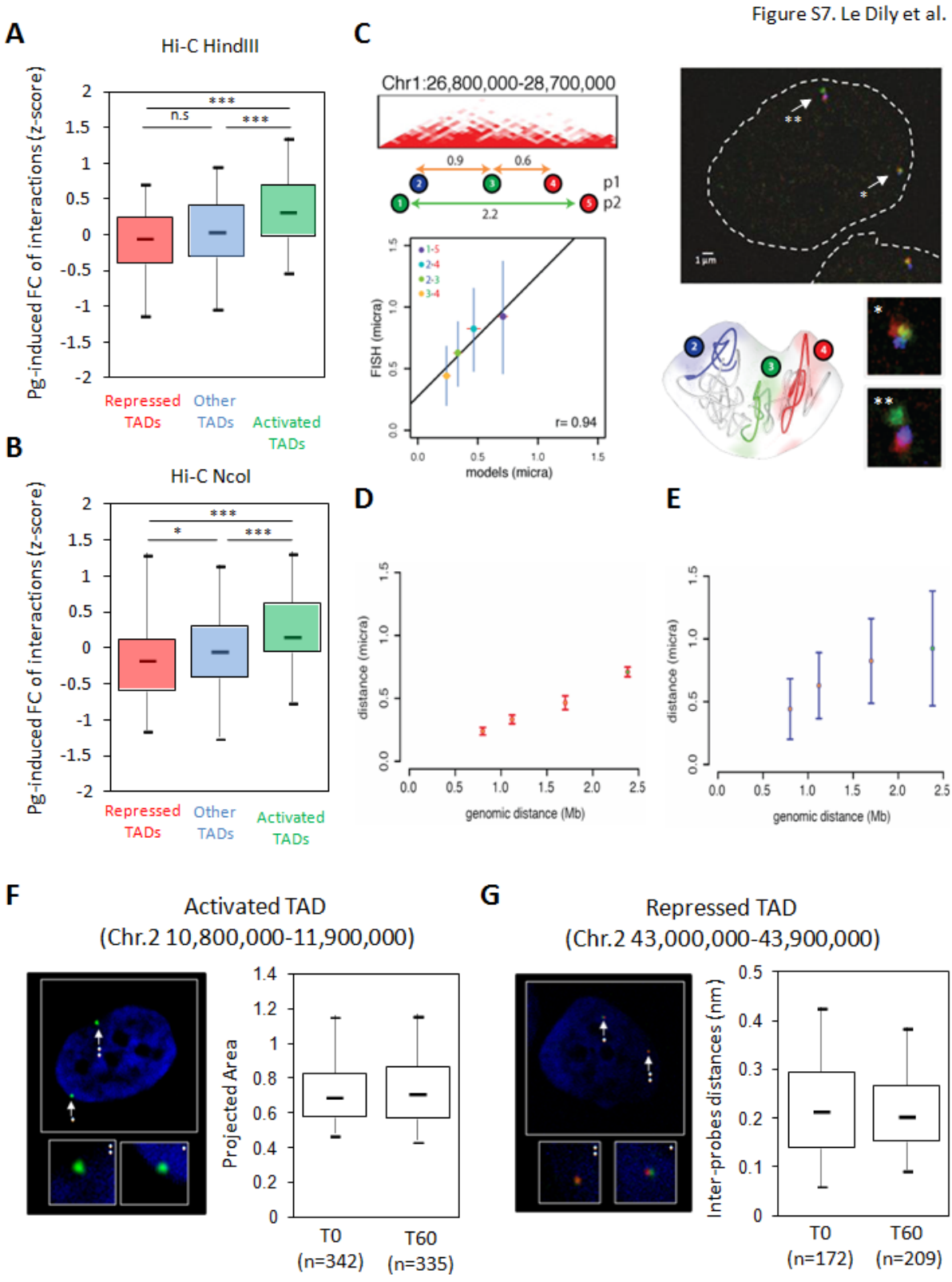

Supplementary Figure 7: Structural changes of TADs.

(A and B) Distributions of the relative changes (z-scores) of intra-TAD contacts proportions upon Pg treatment in the different TAD categories for the two independent datasets obtained with *HindIII* (**A**) or *NcoI* (**B**). Boxplot whiskers correspond to 5st and 95th percentiles. (***),(**),(*) indicate P < 0.001, 0.01 and

0.05, respectively (Bonferroni corrected Mann-Whitney test). **(C)** Two pools of BAC probes located within (p1) or beyond the borders (p2) of a diploid TAD of Chr.1 were used in 3D-FISH experiments (top right image show a representative result obtained with the p1; magnifications are shown below). Virtual 3D-FISH were performed on 3D models of the same region (bottom left panel). The mean and standard deviation of pair-wise inter-probes 3D distances obtained *in situ* (n=60) were compared to the same distances obtained in the 3D models. **(D, E)** Pair-wise inter-probes 3D distances obtained in the models (D) or *in situ* (E) were plotted according the genomic distances that separate them. **(F)** FISH experiments using pools of 4 BAC probes covering around 60% of an activated diploid TADs were performed in T47D cells treated (T60) or not (T0) with Pg and the area of the projected staining was measured. Boxplots show the distributions of the projected area obtained at T0 and T60. The number of individual TADs analyzed for each condition is shown between brackets. **(G)** FISH experiments using 2 differently labeled BAC probes in a repressed diploid TADs were performed in T47D cells treated (T60) or not (T0) with Pg and the inter-probes distances were measured. Boxplots show the distribution of the inter-probes distances obtained at T0 and T60. The number of individual TADs analysed for each condition is shown between brackets.

Figure S1. Le Dily et al.

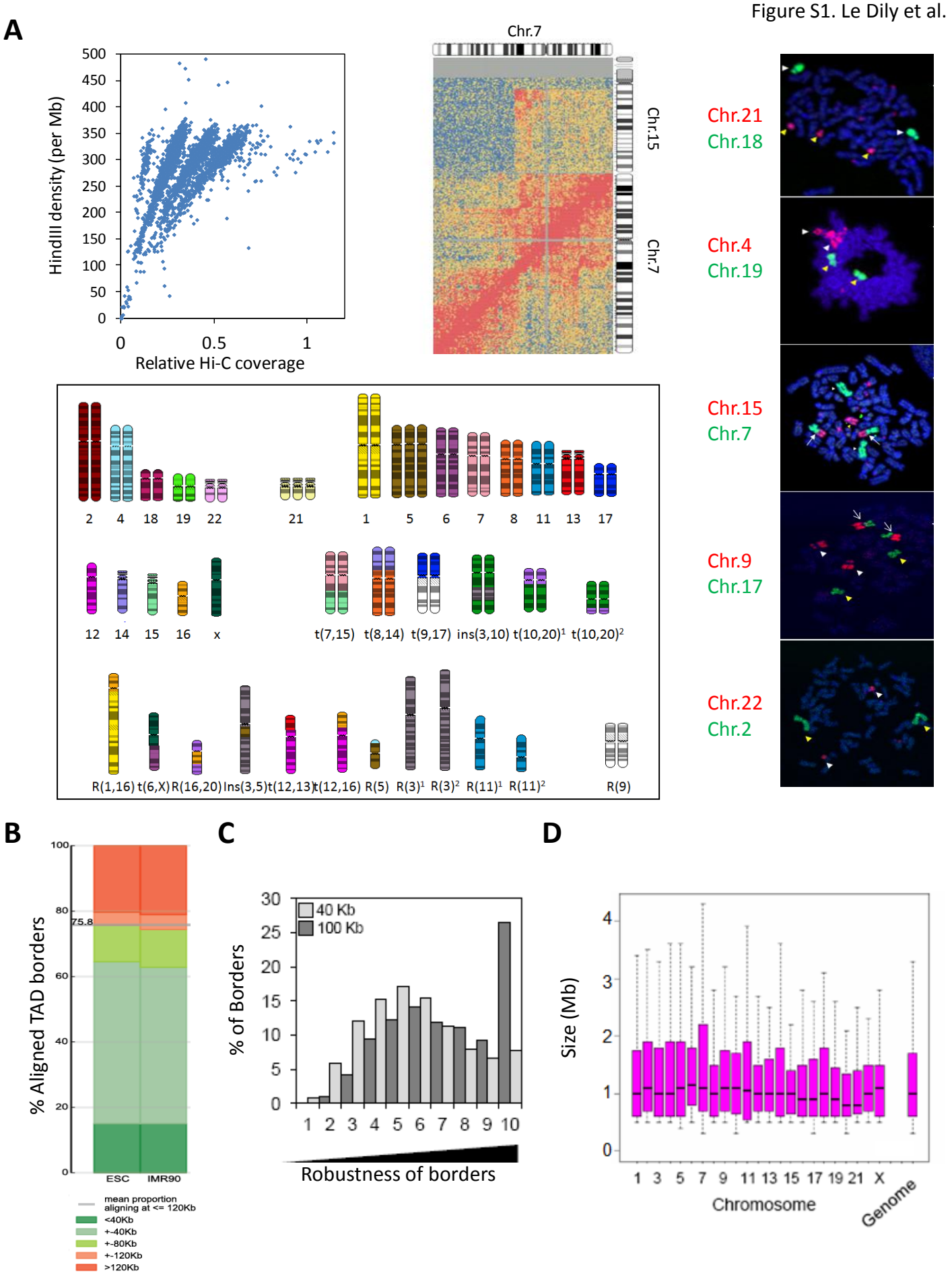

Figure S2. Le Dily et al.

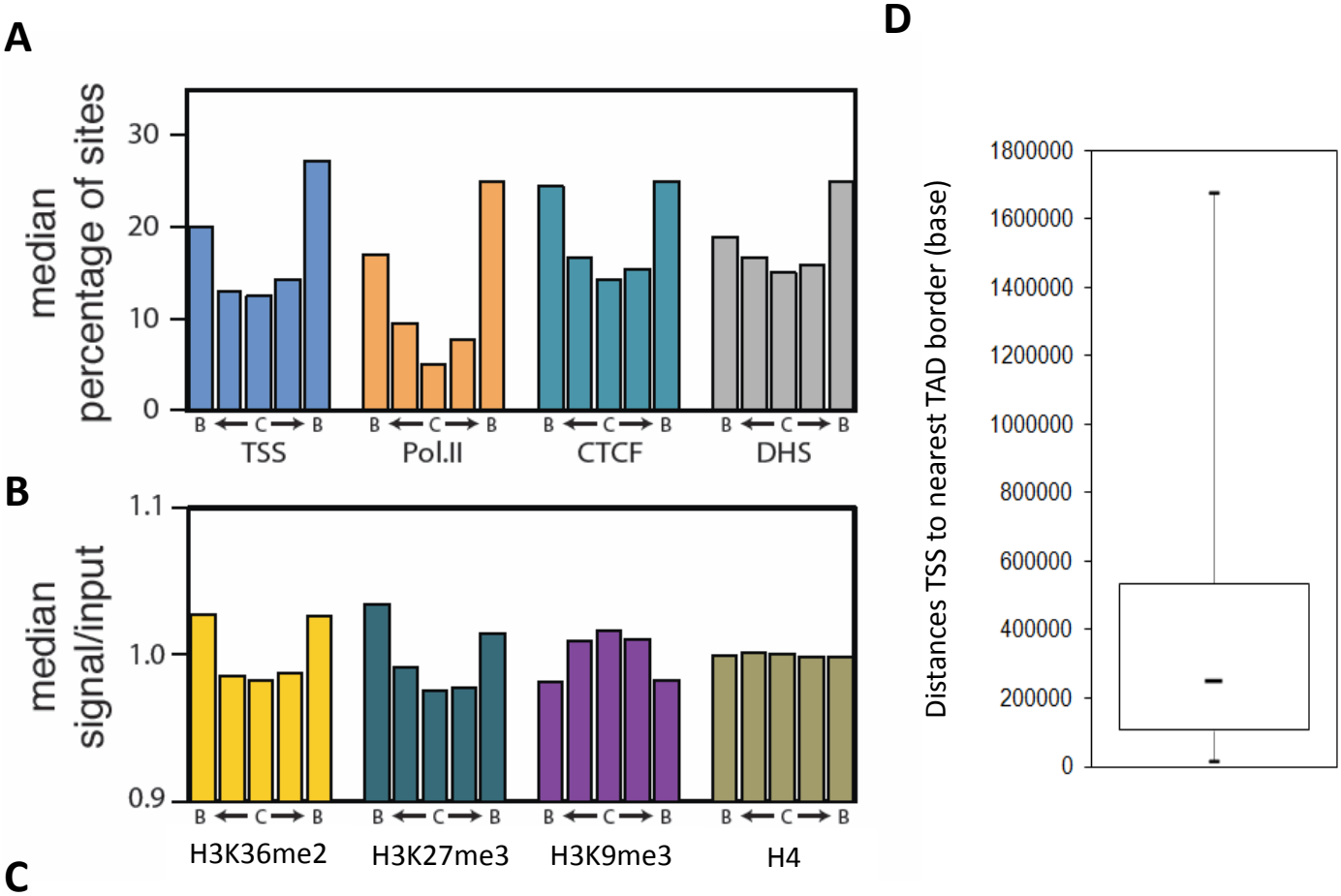

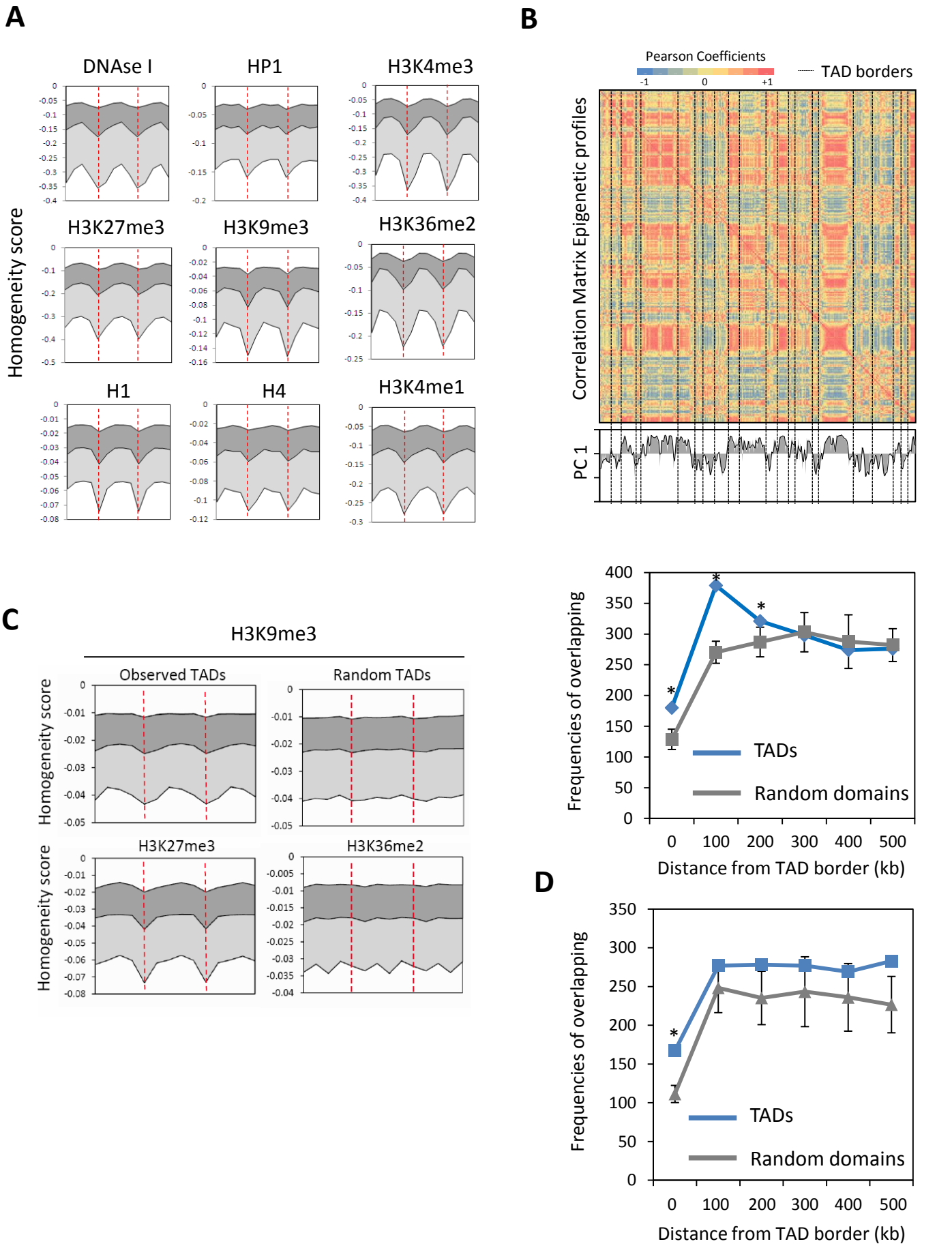
A
DNAse I
HP1
H3K4me3
H3K27me3
H3K9me3
H3K36me2
H1
H4
H3K4me1
Homogeneity score
B
Pearson Coefficients
-1
0
+1
TAD borders
Correlation Matrix Epigenetic profiles
PC 1
Frequencies of overlapping
TADs
Random domains
Distance from TAD border (kb)
C
H3K9me3
Observed TADs
Random TADs
H3K27me3
H3K36me2
Homogeneity score
D
Frequencies of overlapping
TADs
Random domains
Distance from TAD border (kb)

A

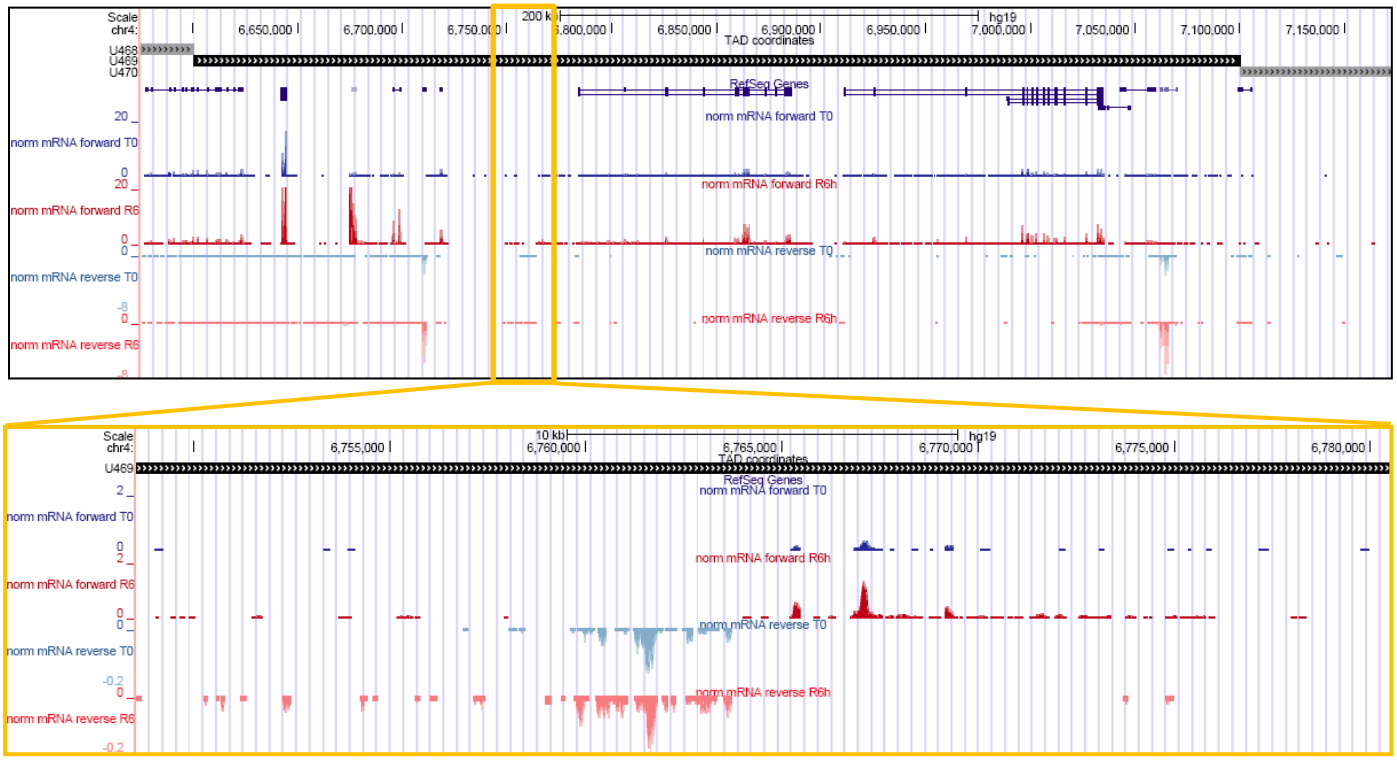
Scale
chr4:
6,650,000
6,700,000
6,750,000
6,800,000
6,850,000
6,900,000
6,950,000
7,000,000
7,050,000
7,100,000
7,150,000
200 kb
hg19
TAD coordinates
U468
U469
U470
RefSeq Genes
norm mRNA forward T0
norm mRNA forward R6h
norm mRNA reverse T0
norm mRNA reverse R6h
Scale
chr4:
6,755,000
6,760,000
6,765,000
6,770,000
6,775,000
6,780,000
10 kb
hg19
TAD coordinates
U469
RefSeq Genes
norm mRNA forward T0
norm mRNA forward R6h
norm mRNA reverse T0
norm mRNA reverse R6h

B

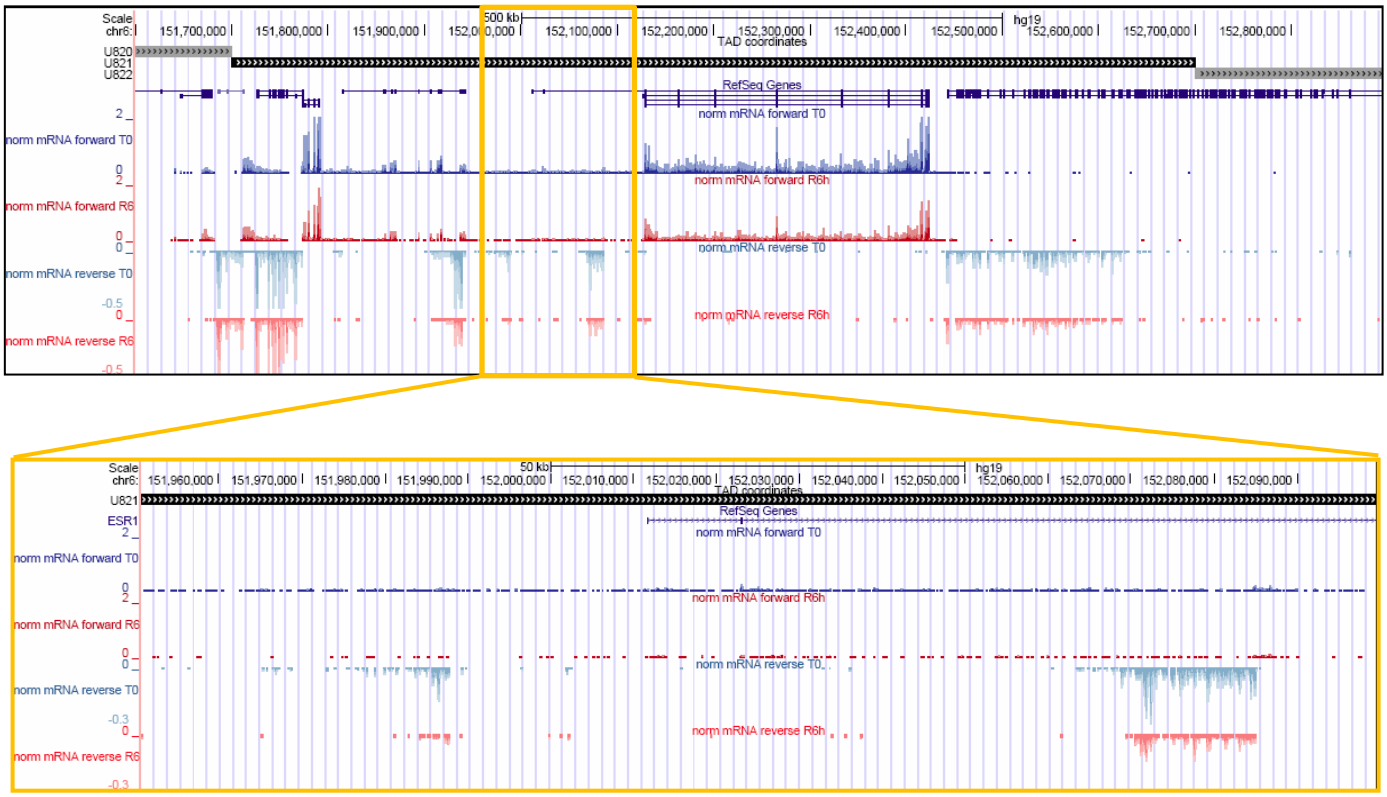
Scale
chr6:
151,700,000
151,800,000
151,900,000
152,000,000
152,100,000
152,200,000
152,300,000
152,400,000
152,500,000
152,600,000
152,700,000
152,800,000
500 kb
hg19
TAD coordinates
U820
U821
U822
RefSeq Genes
norm mRNA forward T0
norm mRNA forward R6h
norm mRNA reverse T0
norm mRNA reverse R6h
Scale
chr6:
151,960,000
151,970,000
151,980,000
151,990,000
152,000,000
152,010,000
152,020,000
152,030,000
152,040,000
152,050,000
152,060,000
152,070,000
152,080,000
152,090,000
50 kb
hg19
TAD coordinates
U821
ESR1
RefSeq Genes
norm mRNA forward T0
norm mRNA forward R6h
norm mRNA reverse T0
norm mRNA reverse R6h

A

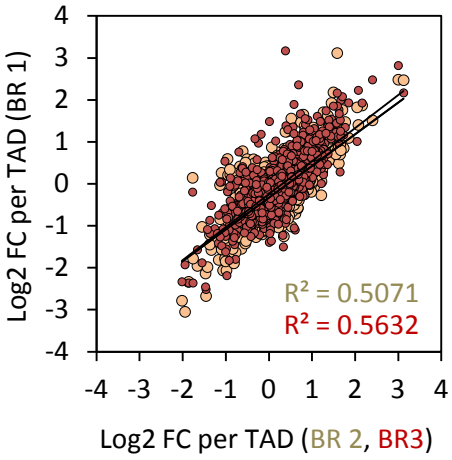

B

		genes	R+ 1h	R- 1h	R+ 6h	R- 6h	E+ 6h	E- 6h
Pg	Repressed	860	14	12	44	153	28	30
	Others	12351	114	67	1162	717	250	127
	Activated	733	32	2	231	36	36	12
E2	Repressed	814	20	7	100	115	5	54
	Others	12143	124	67	1208	716	202	114
	Activated	987	16	7	129	75	107	1

C

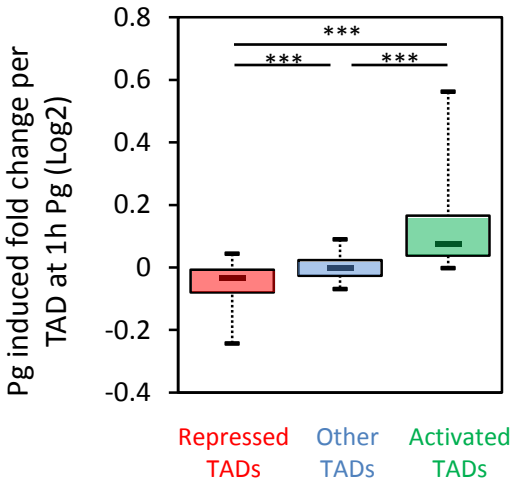

D

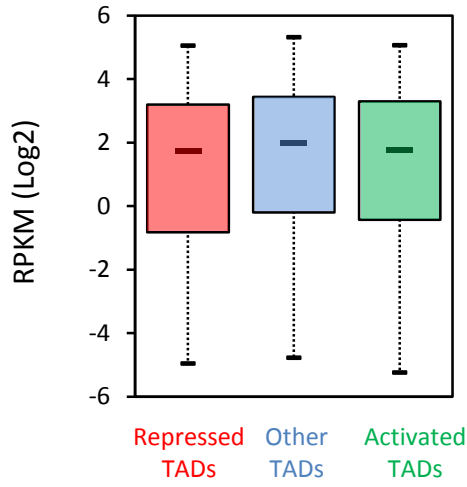

E

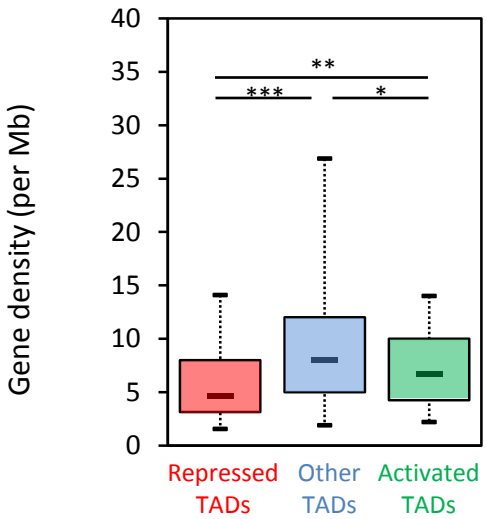

F

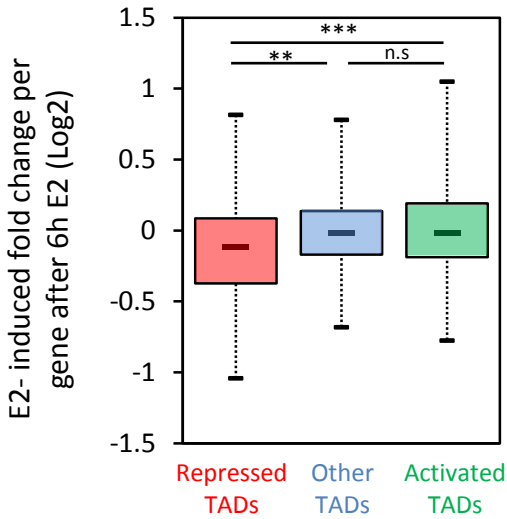

Figure S6. Le Dily et al.

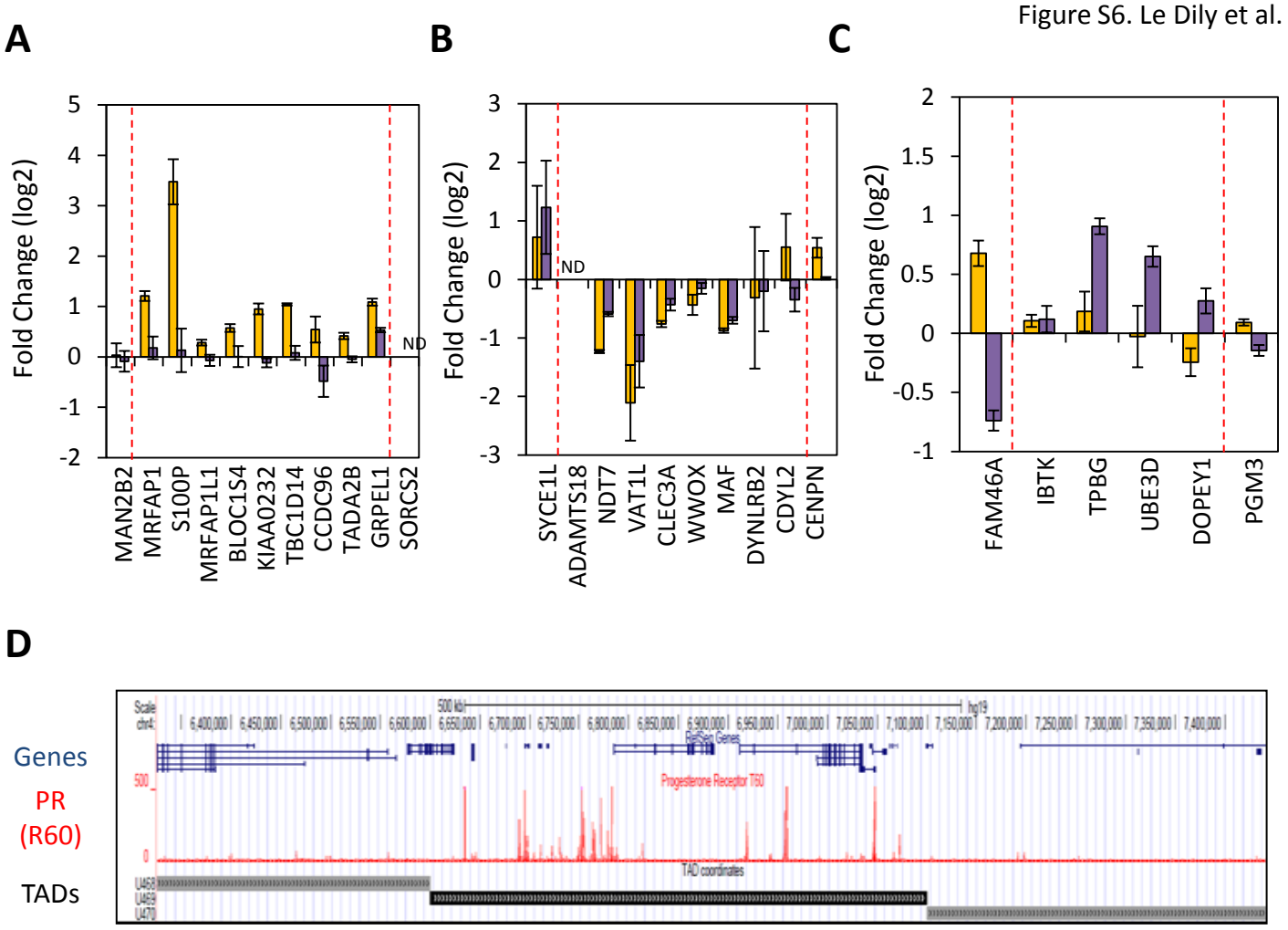

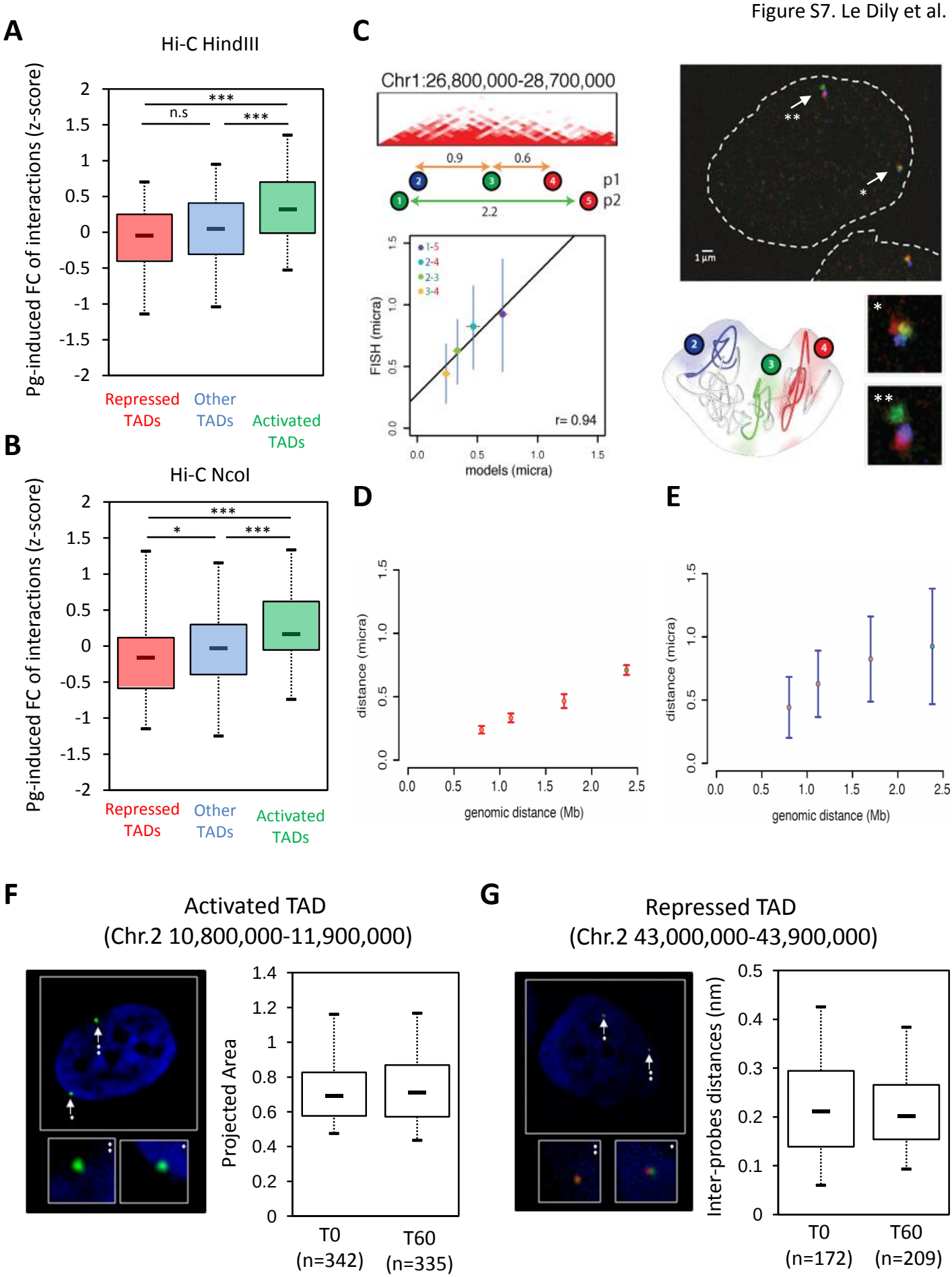
A
Hi-C HindIII
Pg-induced FC of interactions (z-score)
n.s
***
***
Repressed TADs
Other TADs
Activated TADs
B
Hi-C NcoI
Pg-induced FC of interactions (z-score)
*
***
***
Repressed TADs
Other TADs
Activated TADs
C
Chr1:26,800,000-28,700,000
0.9
0.6
2.2
p1
p2
FISH (micra)
models (micra)
r= 0.94
1-5
2-4
2-3
3-4
1 µm
D
distance (micra)
genomic distance (Mb)
E
distance (micra)
genomic distance (Mb)
F
Activated TAD
(Chr.2 10,800,000-11,900,000)
Projected Area
T0
(n=342)
T60
(n=335)
G
Repressed TAD
(Chr.2 43,000,000-43,900,000)
Inter-probes distances (nm)
T0
(n=172)
T60
(n=209)